


RESEARCH ARTICLE | FEBRUARY 21 2019

The thermal effort during marine steam turbine flooding with water **FREE**

Mateusz Bryk ; Tomasz Kowalczyk; Paweł Ziółkowski; Janusz Badur



AIP Conf. Proc. 2077, 020009 (2019)

<https://doi.org/10.1063/1.5091870>



View
Online



Export
Citation

CrossMark



APL Energy

Latest Articles Online!

Read Now

The Thermal Effort During Marine Steam Turbine Flooding With Water

Mateusz Bryk^{1,a)}, Tomasz Kowalczyk^{1,b)}, Paweł Ziółkowski^{2,c)} and Janusz Badur^{1,d)}

¹*Institute of Fluid Flow Machinery, Polish Academy of Sciences, Energy Conversion Department, Fiszerza 14, 80-231 Gdańsk, Poland*

²*Gdansk University of Technology, Faculty of Mechanical Engineering, Department of Energy and Industrial Apparatus, Gdansk, Poland*

^{a)}Corresponding author: mbryk@imp.gda.pl

^{b)}tk@imp.gda.pl

^{c)}pziolkowski@imp.gda.pl

^{d)}jb@imp.gda.pl

Abstract. The work discussed an extreme case of cooling a steam turbine. The ship's steam turbine was used as an example. In marine transport units with low-speed engines dominate, however, there are also units with steam turbines. An example of analysed marine steam turbine is shown in Fig. 1. When considering the issue of cooling steam turbines, it is necessary to estimate the extreme conditions that may occur during operation of the turbine. For this reason, the paper presents the results of the Thermal-FSI analysis of flooding a marine steam turbine with water. The temperature distributions and the corresponding stress fields were determined, which provided information on the effects of flooding the steam turbine with water. New technologies and theoretical examples force a new approach to considered complex flow-strength issues. One of the solutions are calculations that combine liquid and solid, so-called Thermal-FSI (Thermal Fluid-Structure-Interaction). During flow calculations, individual calculated time sub-periods are exported to a solid state solver. Then the problem of the solid body is solved, which results in stresses and deformations. Deformations of geometry result in the subsequent digitization of the geometry. The new grid is passed to the fluid solver in which the next time-stepping is calculated. The operation sequence is repeated until the end of the calculation time.

INTRODUCTION

During the operation of a marine steam turbine the same phenomena occur as in the case of a land-based turbine [1,2]. Although the majority of ship's vessels are equipped with slow-running engines as a propulsion system, it is worth paying attention to vessels with ship's engine rooms with steam turbines.

Different types of turbines (action, reaction, etc.) may require slightly different treatment during start-up, however, the basic principles of start-up are the same for each type of offshore steam turbine, that is:

- lubrication must be ensured
- the turbine must be warmed up properly
- the drainage of the turbine should be opened during the heating process
- the steam boiler must be in good condition and free from waterborne impurities
- the ship's bolt shall be ready for operation
- Cooling water circulation in the capacitor must be switched on [3].

The first issue of the heat-up procedure is to achieve an even rotor temperature. This depends on the small temperature gradient along the rotor shaft, i.e. the rotor temperature must not be higher.

in the top layers than in the deeper layers. If hot steam is applied to a turbine whose shaft does not rotate, the shaft may bend upwards (the so-called cat's back). This will be a natural situation due to the convection that occurs in the dike in the rotor shaft material. Therefore, the rotor must be rotated during heating in order to ensure an even temperature in its entire volume [1,2].

Another issue is to avoid hull warping as much as possible. Again, in this case, the rotation of the rotor causes the steam to mix properly, leading to an even temperature distribution from top to bottom.

The third of these conditions occurs in order to minimize stress caused by the temperature gradient along the thick-walled sectors of the turbine construction. For thick-walled cylinders, if the temperature inside is higher than outside, compressive stresses occur inside the geometry and tensile stresses occur outside. The higher the temperature gradient, the higher the stress values. The same applies to thick and wide flanges at the horizontal points of the bolted connection [1,2,3].

The heat flow from steam to the hull to the bolthole of the flange connection is greatest when steam condenses on the surface, and the temperature at which condensation occurs is determined by the local pressure. The local pressure is in turn determined by the mass flow of steam.

Although it is known that sudden changes in steam temperature in the turbine's flow channel are dangerous for the turbine, it was decided to analyze the extreme case of forced cooling of the turbine - flooding it with water. This situation may occur due to flooding of the ship's engine room. In case of flooding the engine room with a working turbine, the chances of its restarting are negligible, described in the literature. The authors of the study want to determine whether it is possible to reuse the flooded turbine for work.

Flooding of a working turbine with water is an abstract idea, but it may occur. The temperature gradients that occur during such a phenomenon are enormous, which clearly translates into thermal stress and material stress.

ANALYZED GEOMETRY

In this work part of the HP steam turbine from the ship Queen Elizabeth II was analyzed. It is a 12-stage action turbine.

On the basis of Figure 1 a two-dimensional geometry has been prepared, which is shown in Graphic 2. Due to the two-dimensional analysis, the geometry has been simplified accordingly. The flow channel, which is marked in green in Figure 3, was simplified the most.

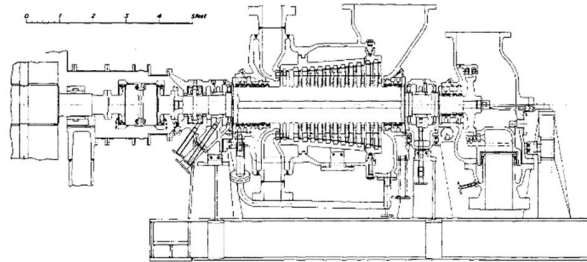


FIGURE 1. Cross-section of the HP part of the steam turbine of the ship Queen Elizabeth II [3].

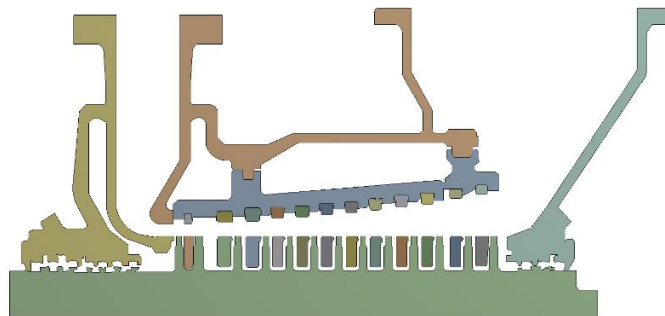


FIGURE 2. 2D model of analyzed geometry.

As it can be seen, the stages of the examined geometry have been simplified. There are no feathers of blades and seals of both steering palisades and rotor palisades. Relieving holes were not taken into account.

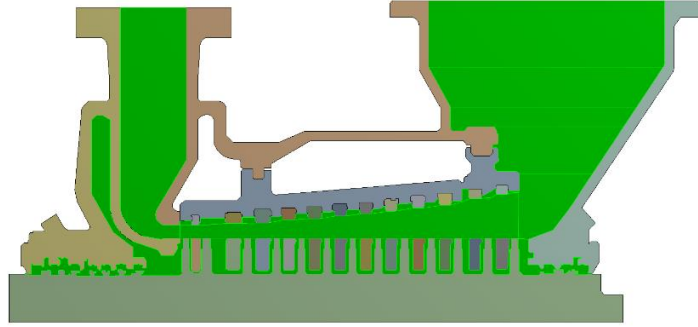


FIGURE 3. Flow channel of analyzed geometry.

Simplification of the geometry is due to the desire to simplify the flow channel. The main focus of the study was on the effect of temperature on solids. Flow has become a secondary issue in the study.

DISCRETISATION

In order to perform both flow and strength calculations, the geometry was discretised using the finite element method. The geometry was discretised by means of square elements. The solid and liquid domain has about 130 thousand elements. A wall layer was applied in the fluid domain. A close-up of the discussed geometry is shown in Graphic 4.

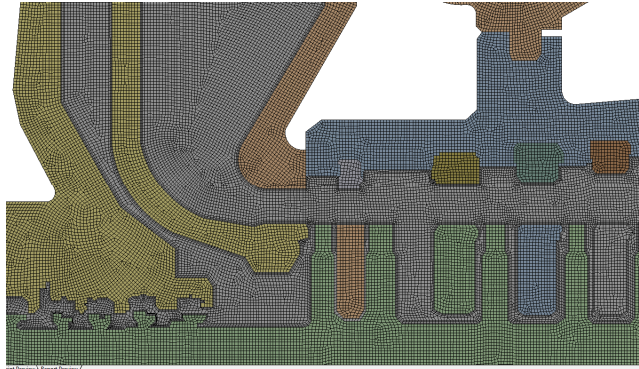


FIGURE 4. Discretisation of the fluid and solid domain.

CFD MODEL

For the fluid flow simulation, three basic formulas of conservation are fulfilled. These three main formulations which describe CFD are presented below [4-6]:

Conservation of mass equation:

$$\partial_t(\rho) + \text{div}(\rho \mathbf{v}) = 0 \quad (1)$$

Conservation of momentum equation:

$$\partial_t(\rho \vec{v}) + \text{div}(\rho \vec{v} \otimes \vec{v} + p \mathbf{I}) = \text{div}(\vec{\tau}^c) + \rho \vec{b} \quad (2)$$

Conservation of energy equation:

$$\partial_t(\rho e) + \text{div} \left[\left(e + \frac{p}{\rho} \right) \rho \vec{v} \right] = \text{div}(\vec{q} + \vec{q}^t + \vec{\tau}^c \vec{v} + \vec{q}^D) + \rho \vec{b} \vec{v} \quad (3)$$



These are balance equations in conservative form, where:

- ρ - gas density, [kg/m³]
- $\vec{\tau}^v = \vec{t} + \vec{R} + \vec{D}$ - total tensor of irreversible stress, [Pa]
- $\vec{v} = v_i \mathbf{e}_i$ - mean velocity, [m/s]
- \vec{q} - molecular heat flux, [W/m²]
- \vec{q}^t - turbulent heat flux, [W/m²]
- \vec{q}^D - diffusive heat flux, [W/m²]
- P - pressure, [Pa]
- $e = u + \frac{1}{2} \vec{v} \cdot \vec{v}$ - total energy, [J]
- $\vec{b} = -9,81 \vec{e}_z$ [m/s²]

Model of turbulence

Above three equation, i.e. (1-3), were complemented by two evolution equations for parameters, which allow to define tensile tensor components [6]:

Evolution equation concerning turbulent energy k :

$$\partial_t(\rho k) + \text{div}(\rho k \vec{v}) = \text{div}(\vec{J}_k) + S_k \quad (4)$$

where,

- k -turbulent energy [J],
- ρ - gas density, [kg/m³],
- $\vec{v} = v_i \mathbf{e}_i$ - mean velocity, [m/s],
- \vec{J}_k - diffusive flux of k , [kg/m²s]
- S_k - k source, [kg/m³s],

Evolution equation concerning energy dissipation ε :

$$\partial_t(\rho \varepsilon) + \text{div}(\rho \varepsilon \vec{v}) = \text{div}(\vec{J}_\varepsilon) + S_\varepsilon \quad (5)$$

where,

- ε - energy dissipation [J],
- ρ - gas density, [kg/m³],
- $\vec{v} = v_i \mathbf{e}_i$ - mean velocity, [m/s],
- \vec{J}_ε - diffusive flux of ε , kg/m²s
- S_ε - , ε sources, kg/m⁴s,

A more detailed description of the used models in CFD codes can be also find in [7]. The pressure of the liquid walls is omitted as a the pressure which causes negligible stress in walls. Because of that, the equation of momentum conservation is not important due to the mechanical reasons but only due to thermal reasons, as the equation which describes heat convection and movement of the hot fluid, which flows through flow channel. For that reason, the viscous and turbulent stress influence is negligible. More important is the assumption of gravity in element of mass force: $\rho(\mathbf{x}, t) \vec{b}$ or a precise equation of water state which gives actual water density in each point and in each moment : $\rho(\mathbf{x}, t)$.

Noteworthy is the heat exchange model in a steam turbine, which is divided into:

- conduction,
- convection,
- radiation.

Due to the considered start-up issue, the most important method of heat exchange is convection between the turbine elements and the steam that is passing them. The second in the process is conduction observed during the whole

turbine operation cycle. The influence of radiation was omitted due to its greatest impact during cooling down of the turbine [8,9]. Therefore, in the formula for total energy (3) radiation was omitted.

CSD MODEL

The following strength hypothesis was used to simulate the stress generated in the material: Huber-Mises-Hencky reduced stress given by formula (6) [5,10,11]:

$$\sigma_{HMH} = \frac{1+\nu}{6E} [(\sigma_1 - \sigma_2)^2 + (\sigma_2 - \sigma_3)^2 + (\sigma_3 - \sigma_1)^2] \quad (6)$$

where,

- ν - number of Poisson
- E - Young's modulus
- $\sigma_1, \sigma_2, \sigma_3$ - main stress

The condition of safe mechanical condition assumes the function (7):

$$\sigma_{red} = \frac{1}{\sqrt{2}} \sqrt{(\sigma_{xx} - \sigma_{yy})^2 + (\sigma_{zz} - \sigma_{yy})^2 + (\sigma_{xx} - \sigma_{zz})^2 + 6(\tau_{xy}^2 + \tau_{yz}^2 + \tau_{xz}^2)} \quad (7)$$

where,

- $\sigma_{xx}, \sigma_{yy}, \sigma_{zz}, \tau_{xy}, \tau_{yz}, \tau_{xz}$ - stress tensor components

or in the equivalent form provided by the formula (8):

$$\sigma_{red} = \frac{1}{\sqrt{2}} \sqrt{(\sigma_{11} - \sigma_{22})^2 + (\sigma_{33} - \sigma_{22})^2 + (\sigma_{11} - \sigma_{33})^2} \quad (8)$$

where,

$\sigma_{11}, \sigma_{22}, \sigma_{33}$ - main stress

Additionally,

$$\begin{aligned} \sigma_{11} &= \sigma_x, \quad \sigma_{12} = \tau_{xy}, \quad \sigma_{13} = \tau_{xz}, \\ \sigma_{21} &= \tau_{yx}, \quad \sigma_{22} = \sigma_y, \quad \sigma_{23} = \tau_{yz}, \\ \sigma_{31} &= \tau_{zx}, \quad \sigma_{32} = \tau_{zy}, \quad \sigma_{33} = \sigma_z, \end{aligned} \quad (9)$$

In order to present the discussed components of the stress state, Figure 5 is quoted.

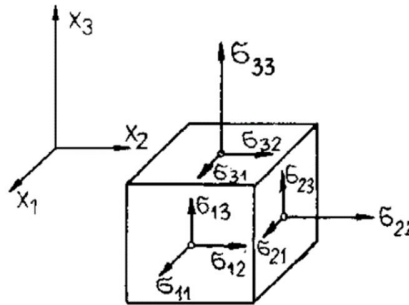


FIGURE 5. Presentation of stress state components [11].

THERMAL-FSI

Thermal-FSI analysis consists in CFD analysis, the results of which are exported to a solid state solver (CSD). Next, the CSD solver on the basis of imported data (temperature, pressure) determines the stress and displacements in the analyzed geometry.

The principle of the analysis is shown in Figure 6.

CFD equations

$$\frac{\partial}{\partial t} \begin{pmatrix} \rho \\ \rho \mathbf{v} \\ \rho e \\ \rho k \\ \rho \varepsilon \end{pmatrix} + \text{div} \begin{pmatrix} \rho \mathbf{v} \\ (\rho \mathbf{v} \otimes \mathbf{v}) + p \mathbf{I} \\ (\rho e + p) \mathbf{v} \\ \rho \mathbf{v} k \\ \rho \mathbf{v} \varepsilon \end{pmatrix} = \text{div} \begin{pmatrix} 0 \\ \mathbf{t}^c \\ \mathbf{J}_k \\ \mathbf{J}_\varepsilon \end{pmatrix} + \begin{pmatrix} 0 \\ \rho \mathbf{b} \\ \rho S_e \\ \rho S_k \\ \rho S_\varepsilon \end{pmatrix}$$

↓ T, P ↑

CSD equations

$$\frac{\partial}{\partial t} \begin{pmatrix} \rho \\ \rho \mathbf{v} \\ \rho e \\ \rho e^{pl} \\ \rho \alpha \\ \rho r \end{pmatrix} + \text{div} \begin{pmatrix} \rho \mathbf{v} \\ \rho \mathbf{v} \otimes \mathbf{v} \\ \rho e \mathbf{v} \\ \rho e^{pl} \otimes \mathbf{v} \\ \rho \alpha \otimes \mathbf{v} \\ \rho r \mathbf{v} \end{pmatrix} = \text{div} \begin{pmatrix} 0 \\ \boldsymbol{\sigma} \\ 0 \\ 0 \\ \mathbf{J}_r \end{pmatrix} + \begin{pmatrix} 0 \\ \rho \mathbf{b} \\ \rho S_e \\ \rho S_{pl} \\ \rho S_\alpha \\ \rho S_r \end{pmatrix}$$

FIGURE 6. Principle of operation of the Thermal-FSI [10].

There are two types of Thermal-FSI analysis [1,5]:

- one way FSI
- two way FSI

In the one way FSI, after CFD calculations, the solution is exported to the CSD solver and the stress and displacements determined on their basis [10].

In the case of two-way FSI analysis, both models (CFD and CSD) are coupled together during the entire simulation. After calculating one CFD time step, the results are exported to the CSD solver. Then, stress and displacement are determined. Then, due to deformations of the analyzed geometry, an automatic remeshing is carried out. The next time step in the CFD solver is calculated with the new mesh. The entire process is carried out automatically until the last time step [12].

The work involved one-way Thermal-FSI analyzes. Temperature fields were imported, from which the stress fields in the analyzed geometry were determined.

BOUNDARY CONDITIONS

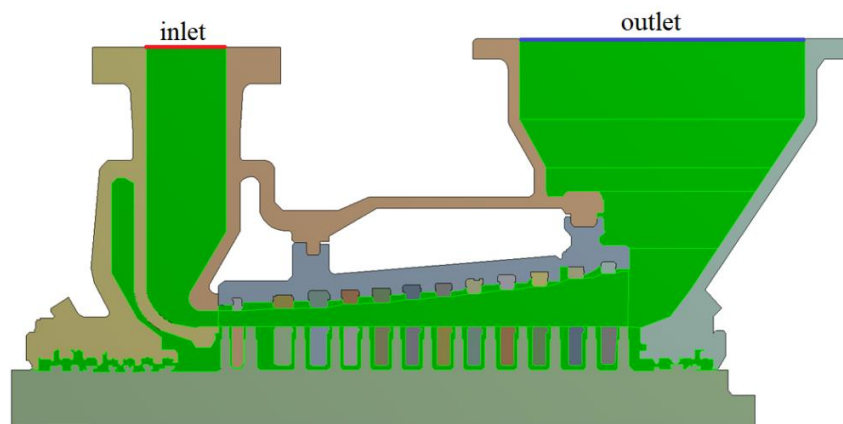


FIGURE 7. Boundary condition for CFD analysis

As a boundary condition, pressure inlet and pressure outlet was set. Graph 7 shows the location of the inlet and outlet from the analyzed geometry. The inlet is marked in red, the outlet is marked in blue. In order to determine the initial state of the turbine for the analysis of its sudden flooding with water, it was necessary to start the turbine. It was a necessary step in order to obtain reliable temperature distributions in the analysed geometry. During commissioning, the steam parameters at the inlet and outlet were implemented according to the actual turbine start-up curves. The

start-up curves of the turbine are presented in Figure 8. Due to the fact that there were no literature data concerning the material data of the turbine construction, it was assumed that it would be made of STg10T steel [1,8,13]. It is a material used in the construction of terrestrial turbines both as a material for the hull and blade.

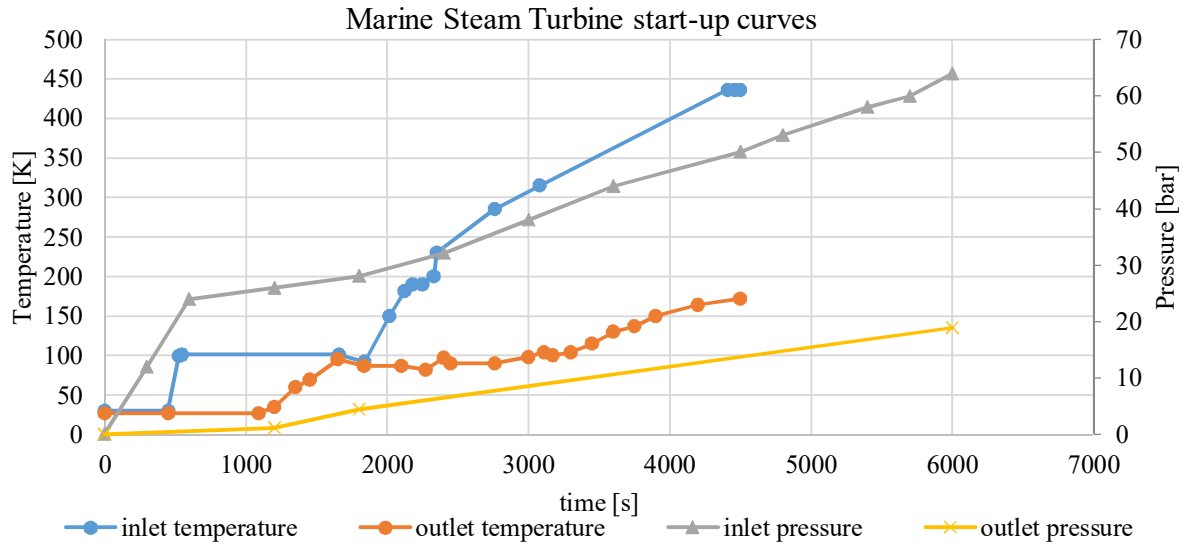


FIGURE 8. Start-up curves for the CFD analysis [3].

Due to the fact that we are dealing with 2D geometry, it was necessary to artificially decrease the enthalpy in the turbine. This was achieved by means of the UDF code, thanks to which the enthalpy drop in particular degrees was achieved.

After bringing the turbine to a steady state of operation, it was flooded with water. The water inlet to the geometry was carried out through the same inlet plane as in the case of commissioning. In the same way, the outlet edge of the geometry remained unchanged. In the analysis, the water has a temperature of 300 K.

CFD RESULTS

The results of the flow analysis are presented in this chapter. The temperature field distributions are presented for each moment of forced cooling. Flow calculations were performed with Ansys Fluent software.

It was decided to show 6 time steps from the simulation, which illustrate the behavior of the temperature field during a sudden flooding of the turbine with water.

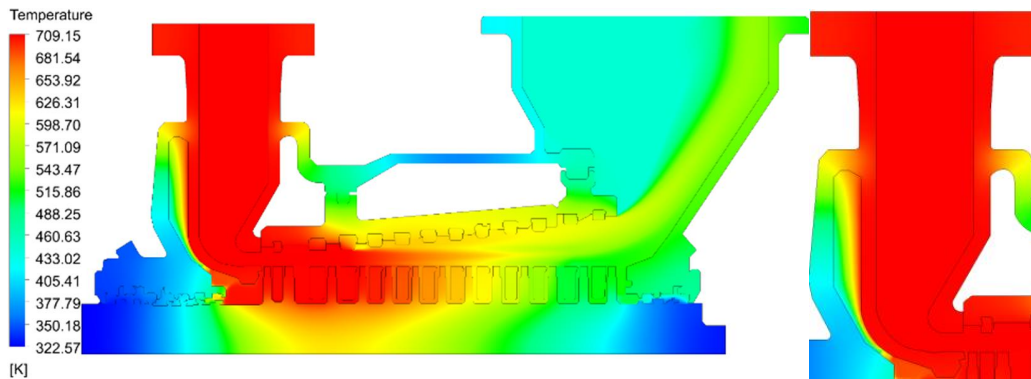


FIGURE 9. Distribution of the temperature field at the final start-up phase of the turbine.

Graph 9 shows the temperature distribution in the final start-up phase of the turbine. This is also the initial temperature distribution for simulating flooding of the turbine. You can see that we are dealing with a standard temperature distribution for the operation of a joint-stock turbine.

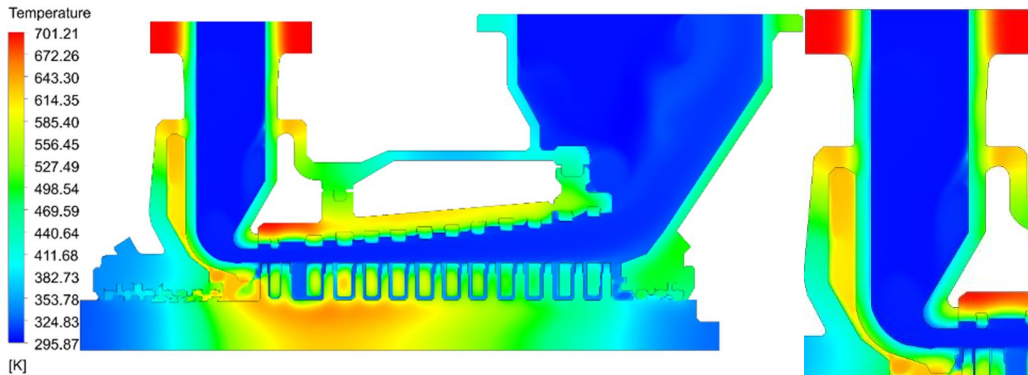


FIGURE 10. Distribution of the temperature field in 46.91 s forced by water cooling.

In 46.91s of forced walking there is a significant cooling down of the turbine structure. The thickest temperature values are found in the thickest elements, i.e. hull flange and turbine rotor. Figure 10 shows the distribution of the temperature field in 46.91s of flooding of the turbine.

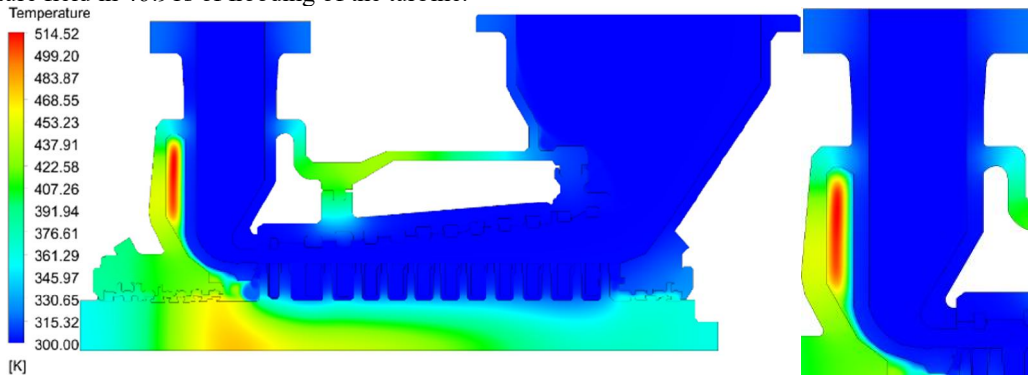


FIGURE 11. Distribution of the temperature field in 1986.91 s forced by water cooling.

Graph 11 shows the final phase of the simulation of flooding the turbine with water. It can be seen that the highest temperature occurs in the space between the inner and outer hull, the outer hull and the rotor. The high temperature value in the space between the hulls is due to the thermal conductivity of the turbine hulls.

The temperature field distributions were used as a reference for the correctness of the calculations performed. Due to the simplification of geometry and flow channel, it can be claimed that the calculations are unreliable. However, due to the fact that it is a steam turbine, the results obtained were referred to the analyses carried out in the works [3,8]. Position [8] treats as a temperature field in the turbine, and position [3] as a temperature field. On this basis, the authors confirm the correctness of numerical calculations. In addition, it should be remembered that more complicated geometry results in longer calculation time and greater complexity of the problem under consideration.

CSD RESULTS

As in the case of flow analysis, the results of the strength analysis are presented in this section. There are presented 5 cases for times 0.01, 0.05, 1.31, 49.61 and 1986.91s respectively. The stresses were determined on the basis of Huber-Mises-Hencky's hypothesis. In the graphs presented, the left side shows the distribution of the reduced stress field H-M-H and the right side shows the radial stresses. The radial stress display shows the nature of the stress occurring.

ROTOR

It was decided not to publish the entire rotor, but the part of the rotor that includes the rotor steps. It was decided to take this step for the sake of better legibility of the results. Strength calculations were carried out using Ansys Mechanical software. The upper part of the graphic shows the stresses H-M-H and the lower part shows the normal stresses.

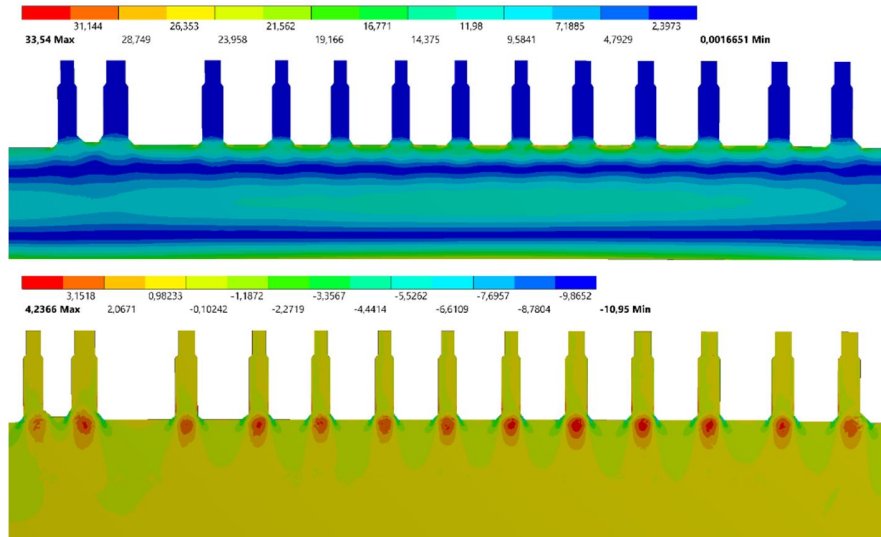


FIGURE 12. Distribution of stress field in the rotor in 0 s forced by water cooling.

Graph 12 shows the distribution of the stress field in 0 s of flooding the turbine with water. Due to the fact that water does not wash the rotor stages, we are dealing with a standard stress distribution in the rotor. The highest value of stress occurring at the moment is 33.5 MPa.

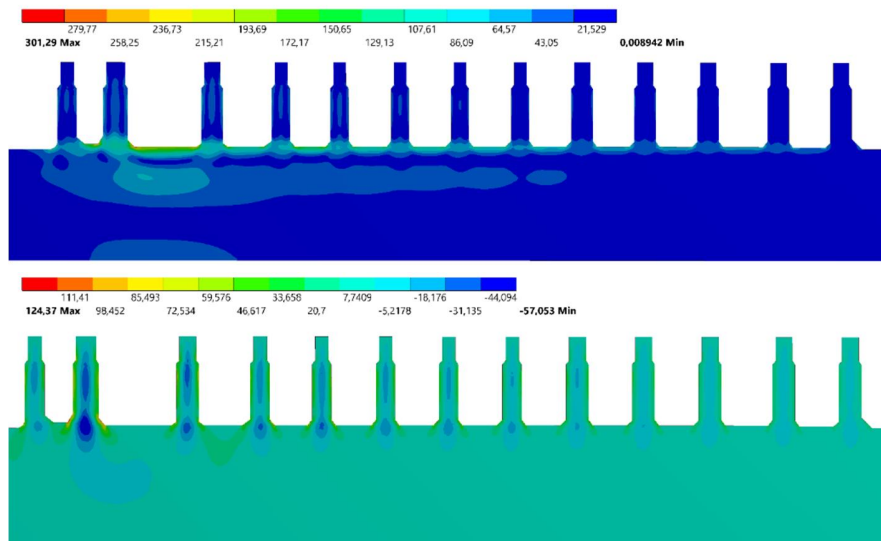


FIGURE 13. Distribution of stress field in the rotor in 46.91 s forced by water cooling.

The distribution of stress field in 49.91 s of flooding the turbine with water is given in figure 13. There is a redistribution of stress field, the value of which drops to 270.9 MPa. After this time the thermal shock passes and the tensile stress drops to 15.9 MPa. The highest values of reduced stress H-M-H are found in the centre of the rotor discs and in the top layers of the rotor.

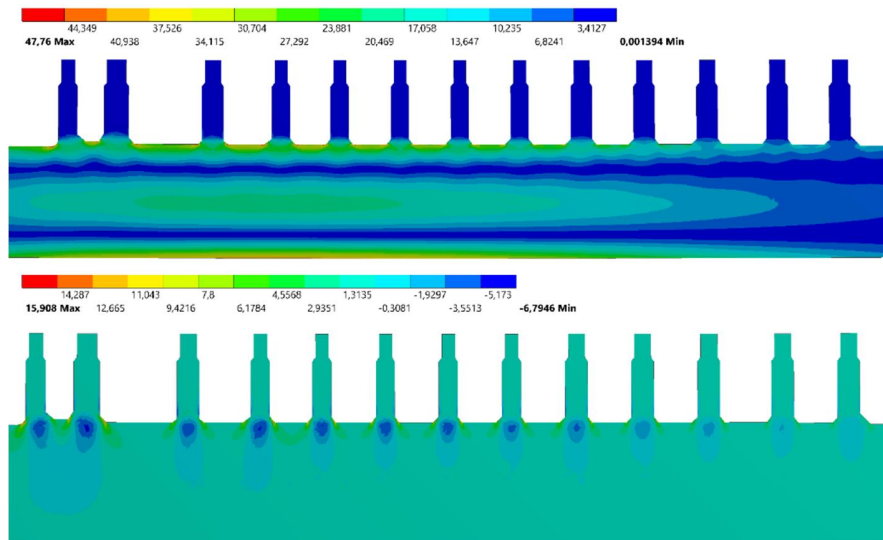


FIGURE 14. Distribution of stress field in the rotor in 1986.91 s forced by water cooling.

Figure 14 shows the stress distribution in the last step of flooding the turbine with water. It can be seen that the stress distribution is analogous to that of the moment before the flooding of the turbine, however, the stress values here are slightly higher than at the initial moment.

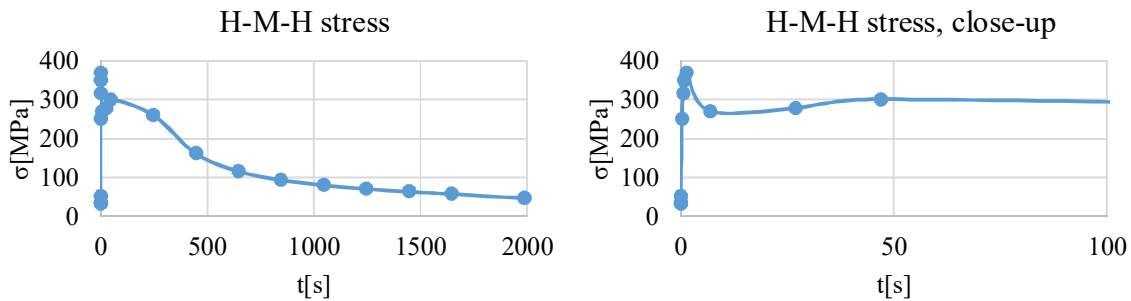


FIGURE 15. The course of stress reduced in the turbine rotor during flooding. On the right side close to the initial phase of forced water cooling.

The course of stress reduced by H-M-H during flooding of the turbine is shown in figure 15. When water enters the flow channel, a thermal shock occurs. The stress in the initial phase rises sharply to 349 MPa. In the next phase, the stress decreases to 251 MPa and begins to rise again to 300 MPa. When the stress reaches 300 MPa, the stress is saturated and reduced. The temperature field equalizes, which leads to a decrease in the stress value in the rotor structure. The initial phase of forced water cooling is presented separately in order to clearly illustrate the stress value course.

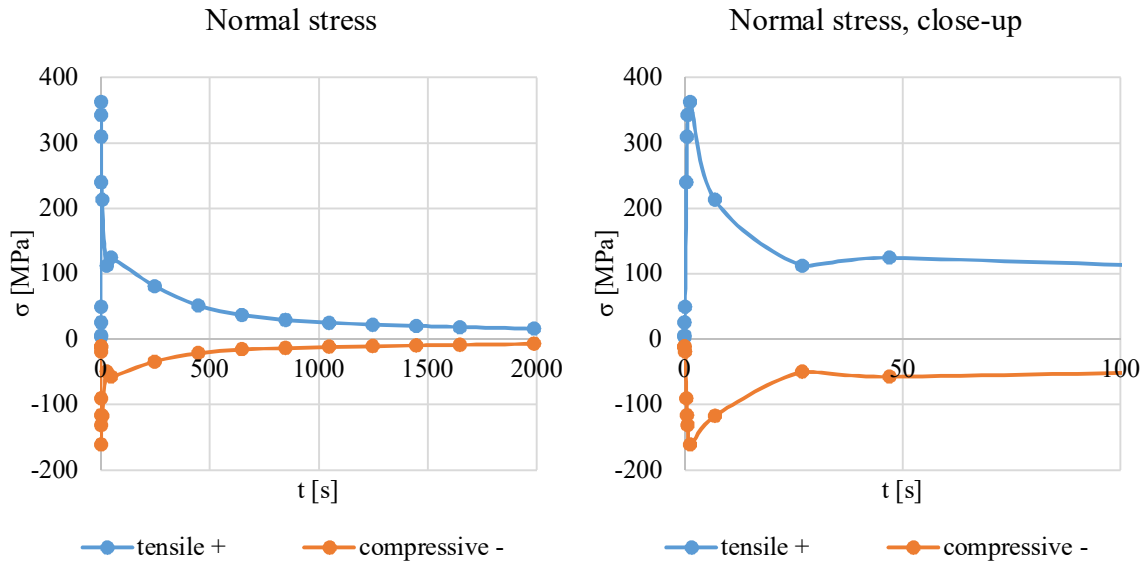


FIGURE 16. The course of radial stress in the turbine rotor during flooding. On the right side close to the initial phase of forced water cooling.

For normal stresses, the same relationship as for reduced stresses is present in Figure 16. In the initial phase the normal stresses rapidly increase to the level of +362 MPa|-161 MPa, after reaching the maximum they decrease their value to the level of +124 MPa|-57 MPa and then there is an equalization of temperatures and decrease of the normal stress value.

As the global stresses in the turbine rotor were considered, the strength analysis was carried out at the rotor points of the most thermally stressed ones. These are points A, B in Figure 17. Point A is marked as pkt 1 and point B is marked as pkt2 on the picture 18.

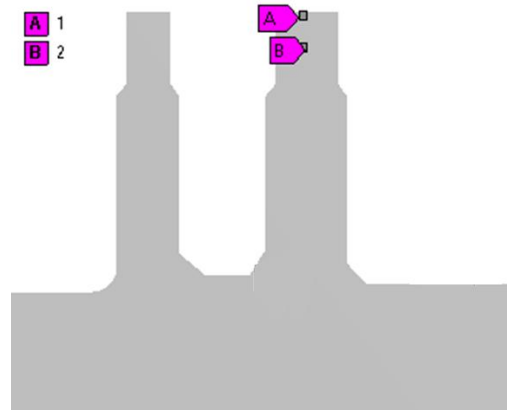


FIGURE 17. Close-up of the analysed turbine rotor area.

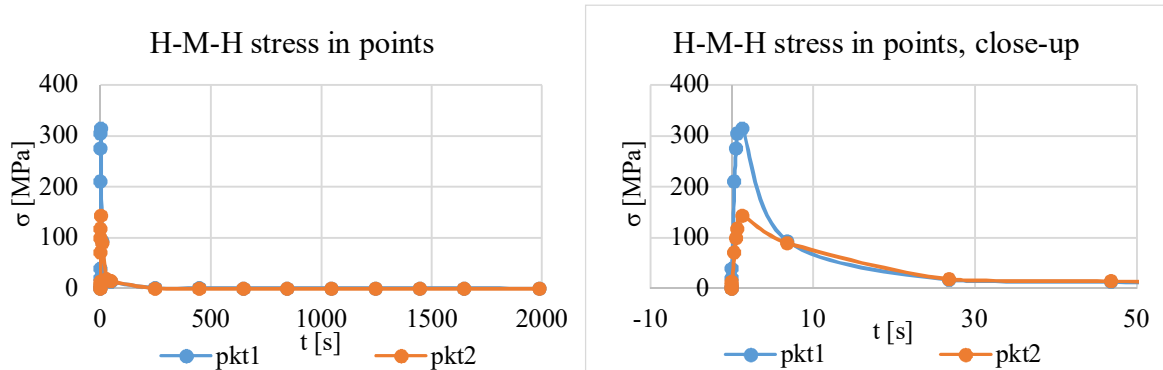


FIGURE 18. Running of stress reduced at two points of the turbine rotor during flooding. On the right hand side a close up to the initial phase forced by water cooling.

Considering the stress values locally, a sudden increase in stress values (thermal shock) is observed, followed by a decrease in stress values to a similar level, which is shown on the figure 18.

HULL

It was decided not to show the whole hull, but its part covering the most heat-stressed parts. The presented part includes both the external and internal hull of the turbine. The results are shown in the graphics from 23 to 31. On the left side of the pictures, the H-M-H stress is shown. On the right side of the pictures, the normal stress is shown.

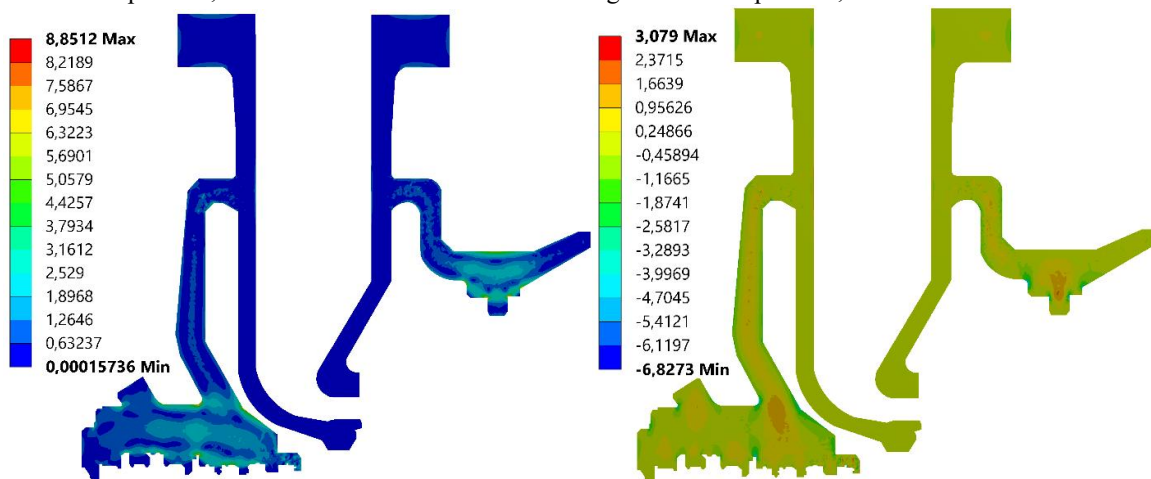


FIGURE 19. The distribution of stress field in the hull in 0 s forced by water cooling.

Graph 19 shows the stress field distribution in 0s of flooding of the turbine. We are dealing with a standard stress distribution after a properly executed turbine start-up. Stress of the highest value occurs at hull joints and in the vicinity of seals in the high-pressure part stress.

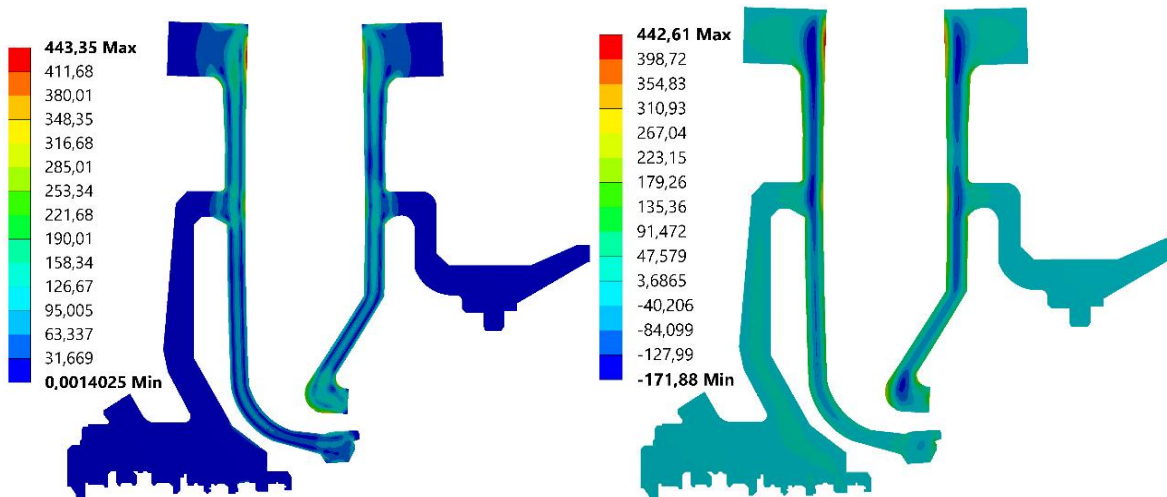


FIGURE 20. The distribution of stress field in the hull in 46.91 s forced by water cooling.

In 46.91s of flooding of the turbine, further redistribution of stress field deep into the hull and flange is observed (Figure 20). Due to the fact that the flange is the thickest element of the hull, stresses are redistributed more slowly than in the thinner elements of the hull. This can be seen on the 26th graph. As in the case of the rotor, the stress value is reduced here too. The maximum value for this time is 443.4 MPa for reduced stress H-M-H and 442 MPa for tensile stress.

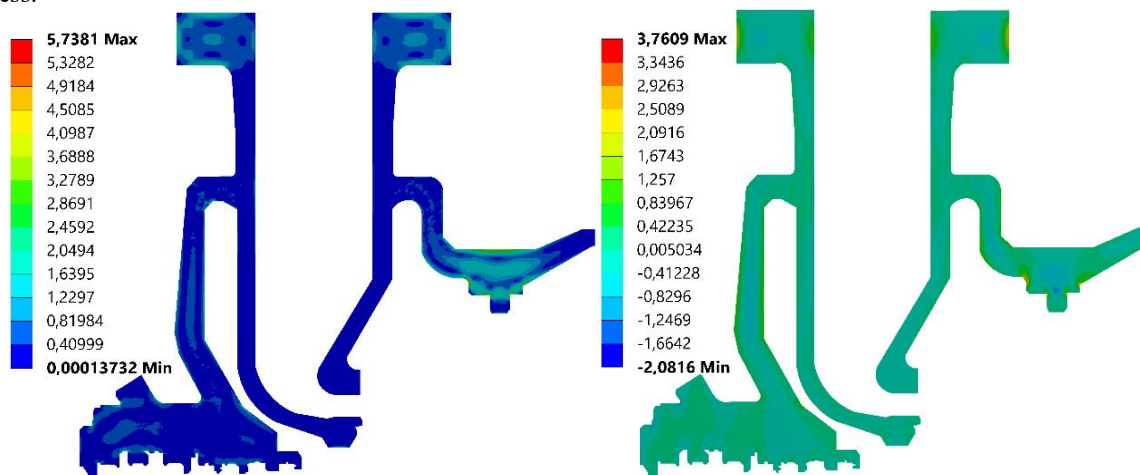


FIGURE 21. The distribution of stress field in the hull in 1986.91 s forced by water cooling.

At the end of the flooding of the turbine, the situation is similar to the initial one. The difference can be seen in the change of the stress field in the flange of the turbine as well as in the vicinity of the seals. The maximum stress remains at the same level as after turbine start-up. Stress values are due to the temperature equilibrium in the hull. It is shown on the figure 21.

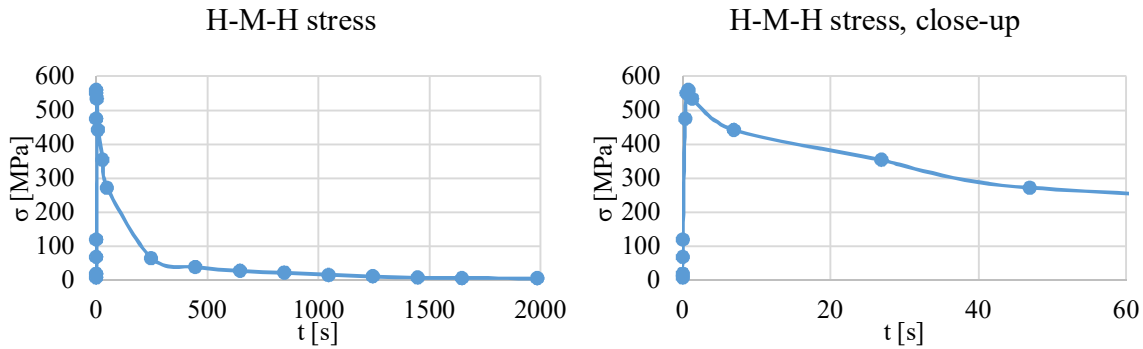


FIGURE 22. The course of stress reduced in the hull of the turbine during flooding. On the right hand side a close up to the initial phase forced by water cooling.

Graph 22 shows the stress relief H-M-H in the turbine hull during forced water cooling. In the initial phase, a thermal shock occurs and the stress increases to 560 MPa in 1.31s. Then the stress is reduced to 5 MPa.

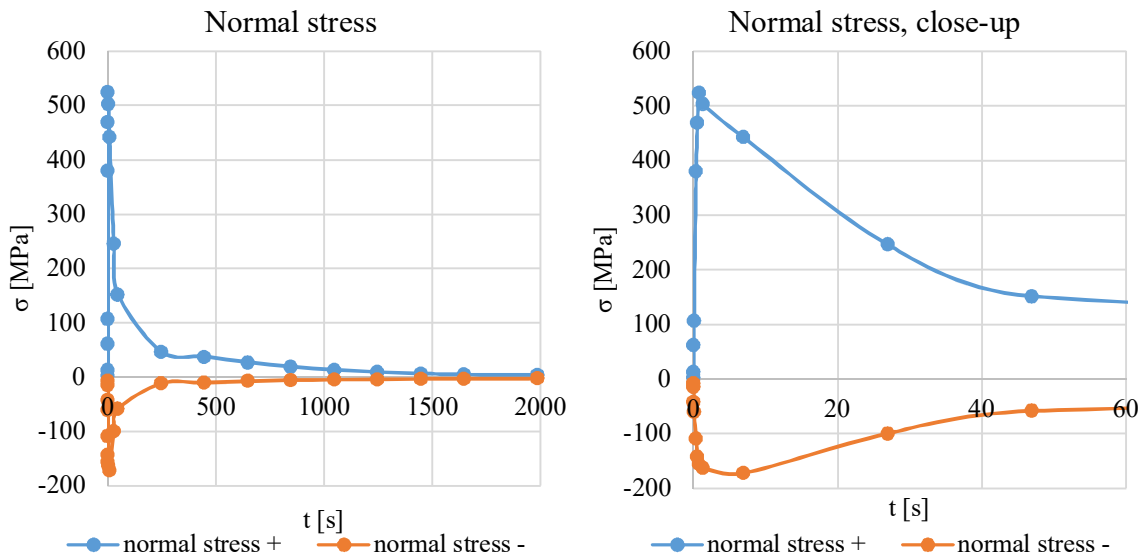


FIGURE 23. The course of radial stress in the turbine hull during flooding. On the right hand side close to the initial phase of forced water cooling.

In the case of normal stress there is an analogy with the reduced stress H-M-H. In the initial phase the stress increases rapidly, with the dominant tensile character. After reaching the maximum within 1.31s (524 MPa) the stresses decrease to 5 MPa. It is shown on the figure 23

As in the case of the rotor, it was decided to make an analysis for selected points of the fuselage most thermally stressed. In this case the stresses on lines A and B of the hull were analysed, which is approximated in Figure 24. Line A is marked as pkt1, line B is marked as pkt2 on the picture 25.

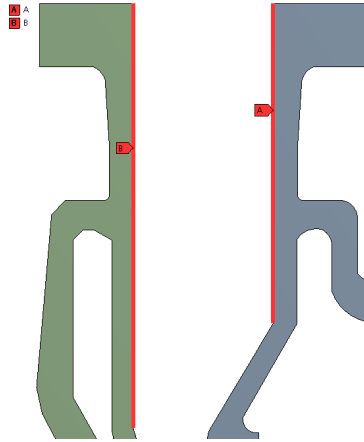


FIGURE 24. Close-up of the analysed turbine hull area.

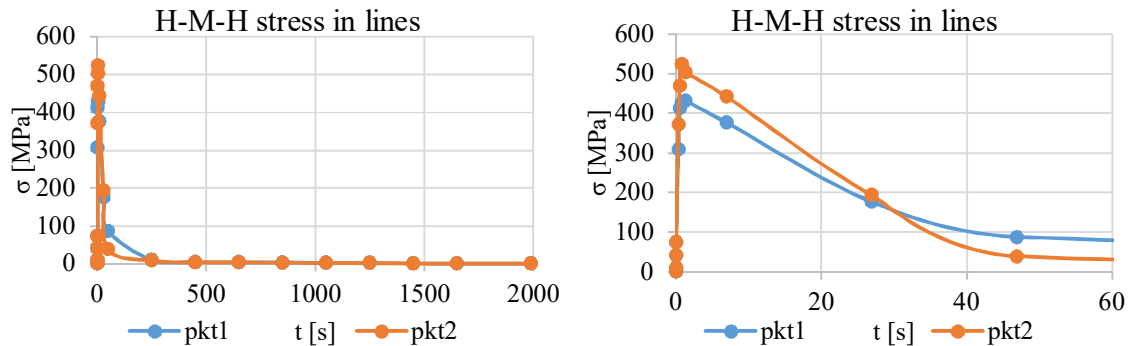


FIGURE 25. The course of stress reduced at two points of the turbine hull during flooding. On the right hand side a close up to the initial phase of forced water cooling.

In the case of the top layer of the hull, a full analogy with respect to the nature of stress shall be observed. Differences occur in the values observed. Higher stress values are found in the analyzed curve 1.

CONCLUSION

The analysis shows that after being flooded, the turbine is not reusable. The strength limit of STg10T at 300°C is 550MPa, at 450°C it is 460MPa. Yield strength at 300°C is 410MPa, at 450°C 370MPa. The creep limit at 300°C is 500MPa, at 450°C 276MPa [13]. Due to high temperature gradients and thermal stress, the strength limit has been exceeded. The material flowed and the yield point was exceeded. Due to the deformation of both the rotor and the turbine fuselage, the elements would be obliterated. In fact, the steps of the turbine would be additionally damaged.

REFERENCES

1. M. Bryk, "Analysis of fast starts up and shut downs of large power steam turbine," Master's thesis, Gdansk University of Technology, Promoter Prof. Dr. J. Głuch, October 2017.
2. M. Banaszkiwicz, "Multilevel approach to lifetime assessment of steam turbines," *International Journal of Fatigue* 73, pp. 39–47 (2015).
3. R. COATS, C.Eng., F.I.Mar.E., M.I.Mech.E., M.R.I.N.A., M.I.Weld., M.N.E.C.I.E.S. Marine Engineering Practice Vol 1, Part 8, Marine Steam Turbines, The Institute Of Marine Engineers.
4. J. Badur, *Numerical modelling of sustainable combustion in gas turbines* (Publishing House of IMP PAN Gdańsk 2003). (in Polish).

5. J. Badur, Bryk M., P. Ziółkowski, D. Sławiński, P. Ziółkowski, S. Kornet and M. Stajnke, "On a comparison of Huber-Mises-Hencky with Burzyński-Pęcherski equivalent stresses for glass body during nonstationary thermal load," *AIP Conference Proceedings* 1822, 020002 (2017); doi: 10.1063/1.4977676.
6. Badur J., *Five lectures on contemporary thermomechanics płynów* (Publishing House of IMP PAN Gdańsk 2005). (in Polish).
7. Badur J., *Development of the concept of energy* (Publishing House of IMP PAN, Gdańsk, 2009). (in Polish)
8. K. Dominiczak, R. Rządowski, W. Radulski and R. Szczepanik, *Neural networks in the steam turbine rotor thermal limitation system*, (Scientific Publishing House of the Institute of Exploitation Technology – PIB: Warszawa; 2015). (in Polish).
9. J. Lipka, *Durability of Rotary Machines*, WNT: Warszawa; 1967 r. (in Polish)
10. P.J. Ziolkowski, P. Ziolkowski and J. Badur, "Unsteady thermal stresses causing plastic flow and the damage of heat-resistant material through the blockage phenomena", in Proc. 11th Int. Cong. On Thermal Stresses, edited by M. Ciarletta et al. (University of Salerno, Italy, 5-9 June 2016), pp. 295 -298.
11. T. M. Huber, Proper deformation work as a measure of material appreciation, *Czasopismo Techniczne* 22, (1904). (in Polish)
12. J. Badur, P. Ziolkowski, W. Zakrzewski, D. Slawinski, S. Kornet, T. Kowalczyk, J. Hernet, R. Piotrowski, J. Felicjancik and P.J. Ziolkowski, "An advanced Thermal-FSI approach to flow heating/ cooling", *Journal of Physics, Conference Series* 530; 2014 pp. 1-8.
13. Bohler steels, <http://www.bohler.de>, (date of access 28.10.2018 r.).